

Physically based assessment of hurricane surge threat under climate change

Ning Lin^{1*}, Kerry Emanuel¹, Michael Oppenheimer², Erik Vanmarcke³

¹Department of Earth, Atmospheric, and Planetary Sciences, Massachusetts Institute of Technology, Cambridge, MA 02139-4307, USA

²Department of Geosciences and the Woodrow Wilson School, Princeton University, Princeton, NJ 08544, USA

³Department of Civil and Environmental Engineering, Princeton University, Princeton, NJ 08544, USA

*Corresponding author, ninglin@mit.edu

Storm surges are very sensitive to the details of storm characteristics as well as coastal geometry and bathymetry; therefore, high-resolution simulations are often required to achieve accuracy in surge modeling. However, any increase of the grid resolution and the associated increase of simulation time steps greatly increases the computational time. High-resolution simulations thus are unsuitable for risk analysis using large storm sets. Fortunately, extreme surge events, which determine the range of risk of concern, are rare events, being only a small fraction of any large set of storms. Therefore, it is critical in surge risk assessment to select the extreme events to be analyzed with high-resolution surge simulations. In this study, we make use of two hydrodynamic models with three grids of very different resolutions to accomplish accurate surge simulations for a group of very large storm sets. The simulations also allow us to compare the models' performances and determine the necessary grid resolution for the study area. Using a relatively small set of extreme storms, we carry out additional simulations to examine the effects on the surge of other related processes, including wave set-up, astronomical tides, and sea level rise (SLR). The results from these investigations, and additional information on the statistical analysis, are presented in this supplemental material.

SLOSH vs. ADCIRC simulations

We compare the storm surges from the SLOSH (with a resolution of ~ 1 km) and ADCIRC (with a resolution of ~ 100 m) simulations in Fig. S1, for two locations within New York Harbor, at the Battery and Staten Island, and two locations close to the entrance of the Harbor, on the New Jersey (NJ) coast and Long Island. The data include 1470 surge events for the NCEP/NCAR 1981-2000 climate condition (results for other data sets have similar trends, not shown); they are selected to be the 10-year and above surge events for the Battery based on the SLOSH simulations. We notice three features in the comparison. First, the simulated surges from the two models are highly correlated, indicating that the SLOSH simulation (using a relatively coarse mesh) is a good filter for this area. Second, the simulated surges from the SLOSH simulations are lower than those from the ADCIRC simulations. This discrepancy is mainly due to the different wind fields applied in the two models. (When we apply the SLOSH wind field to the ADCIRC simulations, the results are not biased relative to those of the SLOSH simulations.) Unlike the wind profile³³ we use in the ADCIRC simulations, which has a defined storm outer radius (~ 400 km) that is consistent with the observed statistics⁴², the wind profile in the SLOSH

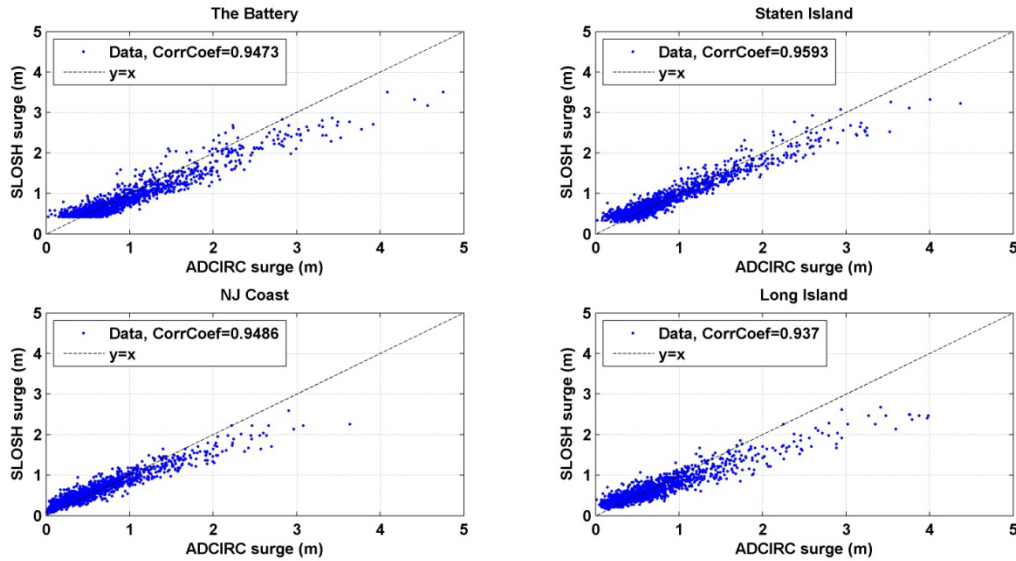


Figure S1. Comparison of the SLOSH and ADCIRC simulated storm surges (1470 events) for four locations around New York Harbor.

model²⁶ is associated with a very long tail (without a well-defined storm outer radius), extending the wind field to large areas and overestimating the storm surges. The surges from SLOSH simulations are actually lower than the surges from the ADCIRC simulations because the SLOSH model assumes a smaller effect of the environmental background flow (often related to storm movement) on the wind field. We add a fraction 0.5 of the translational wind velocity to the entire wind field to account for the asymmetry of the wind field in the ADCIRC simulations; this fraction is determined by a statistical analysis of the observed surface wind fields⁵¹ and storm tracks²² (Chavas 2011, personal communication). The SLOSH model assumes that the magnitude of this effect follows the wind profile, so that it is equal to zero at the center of the storm, increases radially to a maximum of 0.5 times the translational speed at the radius of maximum wind, and then decreases rapidly outward. Since the storm surge is very sensitive to the wind speed near the radius of maximum wind, especially for the extreme events, the SLOSH simulations produce lower surges than the ADCIRC simulations, despite having larger areas of wind effects. Finally, the SLOSH simulations are less sensitive to storm characteristics and often predict similar surges for a range of different storms, compared to the ADCIRC simulations. This lower sensitivity and less successful prediction indicate the effect of the lower resolution of the

SLOSH grid. The differences in applied storm pressure distribution and inflow angle and in model formulation and algorithms may also have contributed to some of the differences in the results.

Effect of grid resolution

In order to determine whether the resolution (~ 100 m) of our ADCIRC grid is sufficient, we apply another ADCIRC mesh³⁰ with resolutions as high as ~10 m around NYC to simulate the 210 most extreme events under the NCEP/NCAR 1981-2000 climate (selected as the 70-year and above events for the Battery based on the ~100-m ADCIRC simulations). (The bathymetric data for the ~10-m mesh were obtained by ref. 30 from the NOS database of the coastal hydrographic surveys, the U.S. Army Corps of Engineers nautical charts, and multibeam data collected by Stony Brook University ship surveys; the bathymetric data of the ~100-m mesh are obtained by interpolation from the ~10-m mesh.) The comparison of the simulated surges using these two grids is shown in Fig. S2 for the four locations around New York Harbor. The differences between the results are very small, with our relatively coarse mesh on average overestimating the surge at the Battery by about 2.5% and at the NJ coast by about 1% and underestimating the surge at Staten Island and Long Island by less than 3%. The smallness of the differences indicates that the resolution of a few hundred meters around NYC is sufficient for accurate surge simulations. More significantly, using the ~100-m mesh greatly reduces the computational time (by about 25 times compared to using the ~10-m mesh), making large numbers of simulations for risk assessment possible and efficient. Therefore, we use the ~100-m ADCIRC simulations to assess the surge probabilities for the Battery, with a simple 2.5% reduction of the surge magnitude to account for the effect of the grid resolution.

Effect of wave set-up

Storm surges are accompanied by wind waves, which induce wave set-up due to radiation stresses (the flux of momentum carried by the waves). In order to investigate the effect of the wave set-up on the surge level, we also simulate the selected 210 extreme events with the ADCIRC model³² that is coupled with a SWAN spectral wave model⁵², using the ~100-m ADCIRC mesh. The comparison of the surge levels with the wave set-up simulated by the

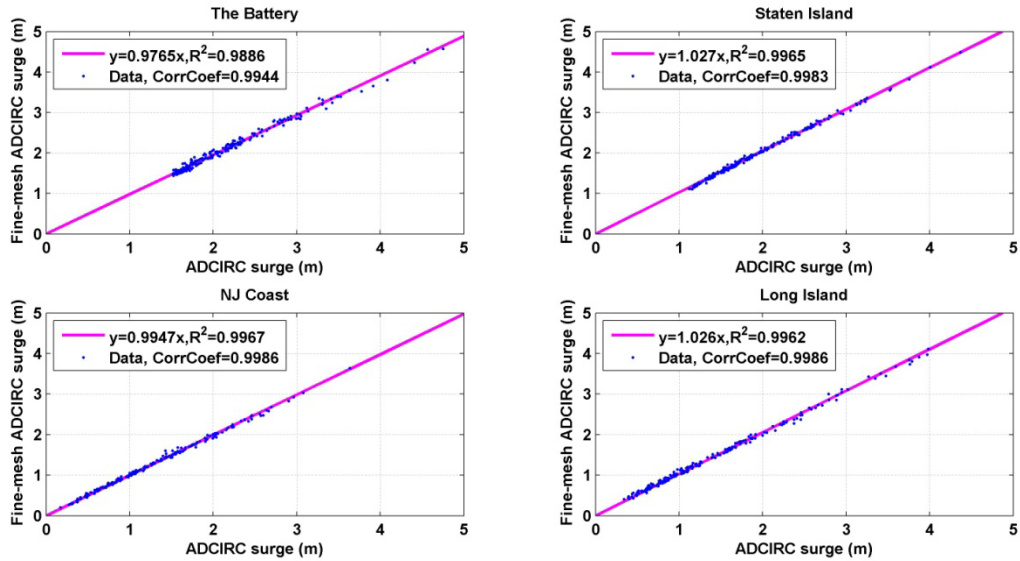


Figure S2. Comparison of the ADCIRC simulated storm surges (210 extreme events) using the ~100-m mesh (x axis) and the ~10-m mesh (y axis), for four locations around New York Harbor. The magenta line represents the linear regression of the data.

ADCIRC+SWAN model and the surge levels simulated by the ADCIRC model is shown in Fig. S3. The wave set-up is found to be small (less than 1.5% of the surge) for the four locations around New York Harbor. To check the effect of the grid resolution on wave simulations, we also applied the ~10-m ADCIRC mesh for the top 10 extreme events and found the wave set-up to be similar or smaller (not shown). The smallness of the wave set-up in the NYC area may be due to the fact that the large ocean waves break before entering New York Harbor⁴¹. Also, since both of these meshes are confined to the open ocean and they do not include any land, some details of the near-shore wave breaking may not be captured. Nevertheless, given the topography and bathymetry of the study area, the wave set-up is estimated to be small (Westerink 2011, personal communication). Therefore, we neglect the wave set-up in this case, considering also that wave simulations are computationally intensive (with the computational time for the surge-wave-coupled simulation more than 10 times that for the surge simulation in this case). (Note that the magnitude of wind waves can be very large for extreme surge events, with the significant wave height up to 5-6 m for the Battery, but it does not affect the mean surge level considered in this study.)

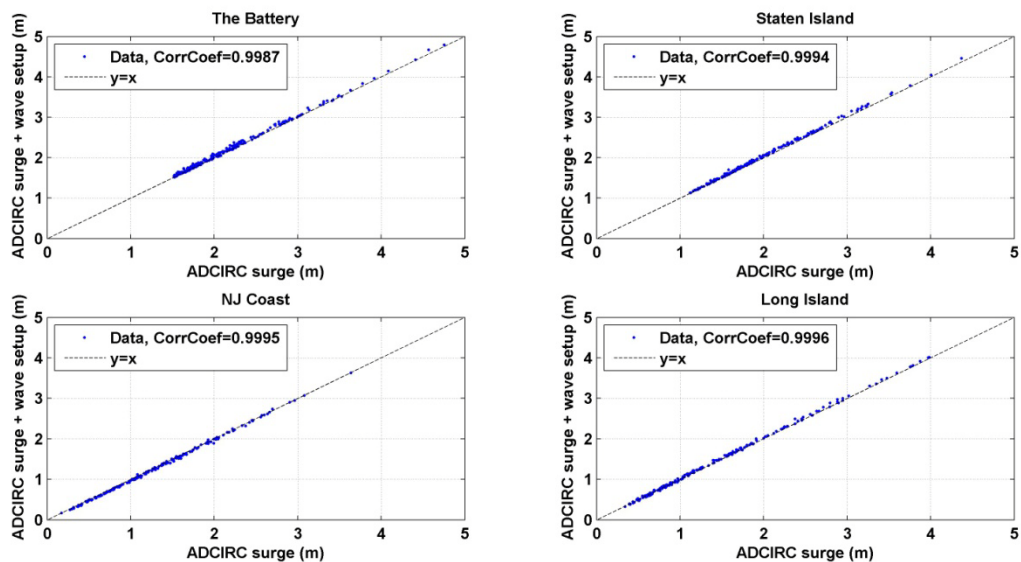


Figure S3. Comparison of the ADCIRC simulated surges (210 extreme events) without (x axis) and with (y axis) the wave set-up, for four locations around New York Harbor.

Effect of astronomical tide

Storm surges can happen at different phases of the astronomical tide. The total water level above mean sea level, due to the combined effects of the storm surge, wave set-up, astronomical tide, and riverine flow, is referred as the storm tide. When the effects of wave set-up and riverine flow are small (as for the NYC area), the storm tide may be estimated as the combination of the storm surge and astronomical tide. If the interaction between the surge and astronomical tide is small, the storm tide is approximately the linear superposition of the two. However, we notice that the tide-surge nonlinearity (L) is relatively large, with a mean absolute value of about 9% of the surge (and 60% of the tide magnitude) for the Battery. The tide-surge nonlinearity has been observed by previous studies, and it is attributed to nonlinear effects of the bottom friction and momentum advection on the surge due to the presence of the tide^{53,54}. In order to quantify this nonlinearity over a tidal cycle, we simulate the storm surge and storm tide, for each of the 210 extreme events, every 3 hours during a day in a hurricane season. The results show that a storm surge tends to be reduced ($L < 0$) when it happens at the high tide or during the rising tide, while it

tends to be increased ($L>0$) at the low tide or during the receding tide, as shown in Fig. S4 for the Battery (the patterns are similar for other locations around New York Harbor, not shown).

This pattern leads us to model the tide-surge nonlinearity as a function of the tidal phase, as well as the surge height, tidal range, and mean tidal level. (As simulations of the storm tide are computationally expensive, using empirical methods to account for the tide-surge nonlinearity is necessary in risk assessment.) We define the non-dimensional factor γ for the nonlinearity (see Methods in the main article), calculate its value for all the simulated surge events, and model its mean (over the events occurring at each half hour) by kernel regression as a function of the tidal phase, as shown in Fig. S5. The obtained function γ can be used to estimate the nonlinear effect on the surge of any given tide for the study area. For example, the model-simulated tide matches the observed tide relatively well in phase, but less well in terms of the tidal range and mean tidal level (Fig. S5). In such a case, we may use the γ function, which is modeled based on the simulated tide, to predict the nonlinear effect of the observed tide, using the observed tidal range and mean tidal level.

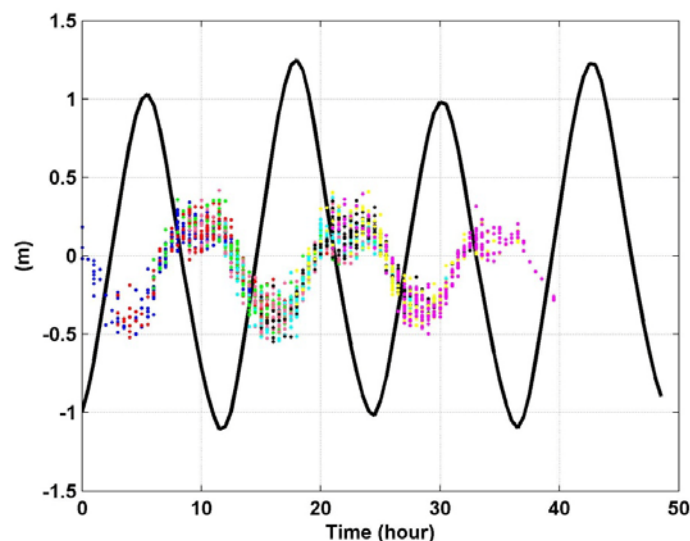


Figure S4. Simulated astronomical tide (black curve) and the tide-surge nonlinearity (dots; the difference between simulated storm tide, surge, and astronomical tide), for 210 extreme events happening every 3 hours during a day. Each color of the dots represents a set of 210 events; 8 sets are shown. The simulated astronomical tide is for the period of 18-19 September 1995.

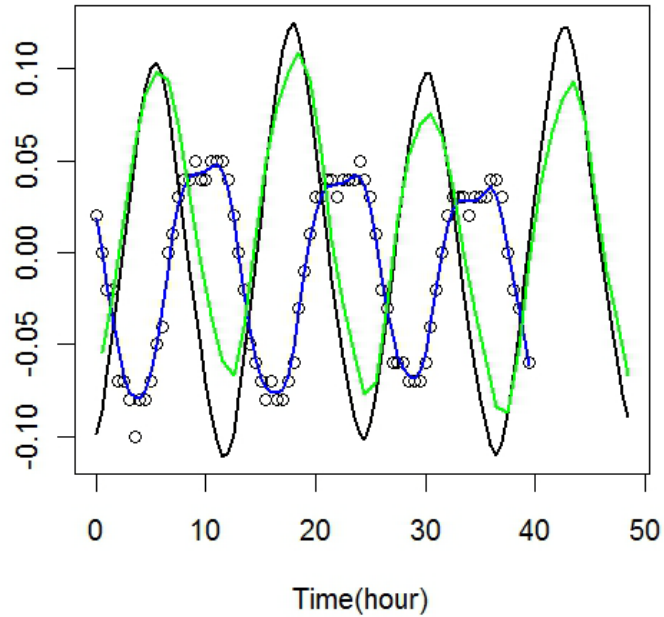


Figure S5. Regression (blue curve) of the average nonlinearity factor γ (open circles), together with the simulated astronomical tide (black curve) and the NOAA observed tide (green curve). The simulated and observed astronomical tides are for the same period of 18-19 September 1995; the magnitudes of the tides (m) are scaled by 1/10.

Effect of sea level rise

The storm surge and storm tide levels are relative to the mean sea level. As the sea level will rise due to the global warming, it is necessary to check whether the surge will be affected by SLR. We perform another set of ADCIRC simulations for the 210 extreme events with the mean sea level increased by a range of possible values predicted for NYC for the end of the century⁴⁰. As shown in Fig. S6, the nonlinear effect of the SLR on the surge (the difference between the simulated surge above the raised sea level and the simulated surge above the present sea level) is very small for the Battery (and for the other locations around New York Harbor, not shown), especially for the most extreme events and when the SLR is lower than 1 m. This effect is larger when the SLR is greater than 1.5 m, but it fluctuates almost symmetrically around zero; thus the net effect is statistically small. This smallness of the observed effect is consistent with the first-order theoretical estimation that the magnitude of the SLR effect is mainly determined by the ratio the SLR to the coastal bathymetry, which is often very small⁴⁹. This SLR effect may thus be

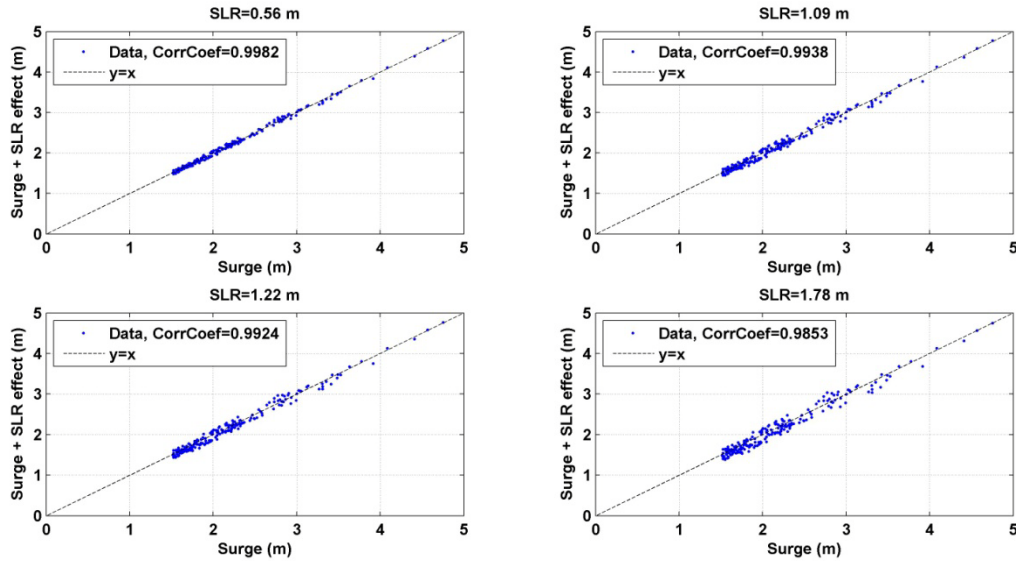


Figure S6. Comparison of the ADCIRC simulated surges (210 extreme events) without (x axis) and with (y axis) the effect of SLR at the Battery, for four SLR levels (0.56 m, 1.09 m, 1.22 m, and 1.78 m).

neglected; therefore, the projected SLR in future climates can be accounted for linearly when estimating the flood height including the storm tide and SLR.

Statistical assumptions

The annual number of tropical cyclone genesis events has been shown to be approximately Poisson-distributed^{55,56}. Based on the theory of Poisson random measure, it can be mathematically proved that, under reasonable assumptions, the Poisson characteristic of storm genesis leads to the Poisson characteristic of hurricane landfall over any coastal sections, over any temporal segments (for example, El Niño years), and/or with any intensity range (for example, intensity greater than Category-3 level). These theoretical Poisson features are consistent with observations (see Fig. S7 and, for example, ref. 57). Therefore, we assume the annual number of tropical cyclones that pass by a surge site with an intensity over a threshold to be Poisson-distributed, with mean λ . In this study, λ is the annual frequency of NY-region storms (storms that pass within a 200-km radius of the Battery with a maximum wind speed greater than 20 m s⁻¹). Let the level of annual maximum storm surge be H_{max} , and then the probability

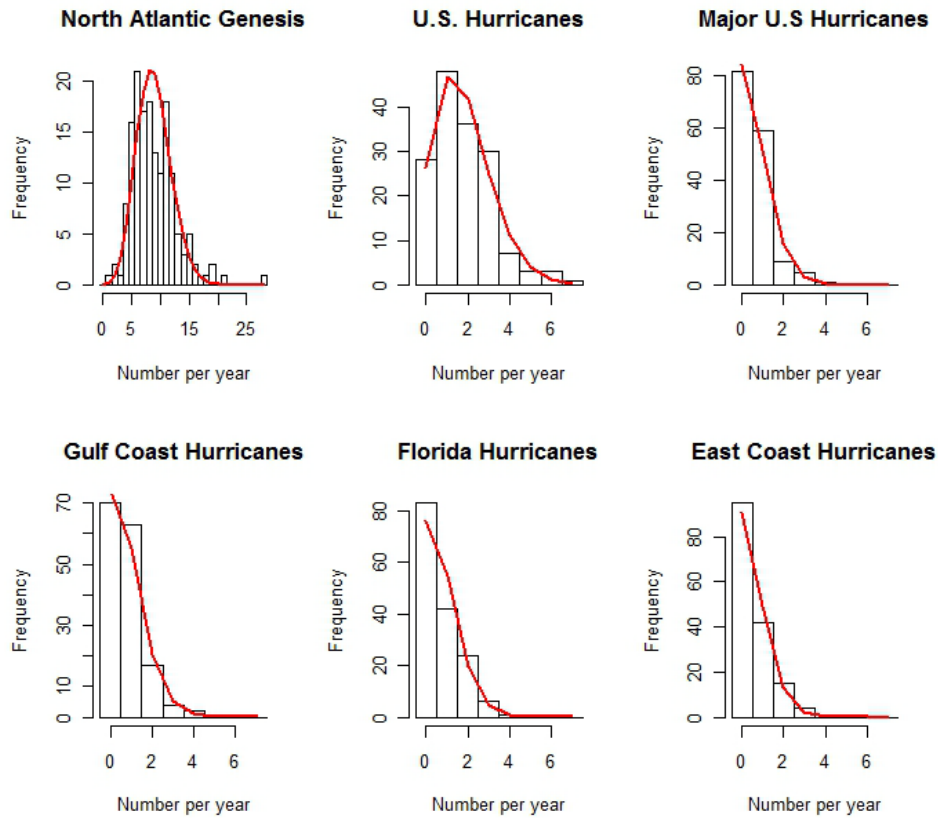


Figure S7. Histograms of the observed counts of North Atlantic genesis, U.S. hurricanes, major U.S. hurricanes, Gulf Coast hurricanes, Florida hurricanes, and East Coast hurricanes, with the fitted Poisson distribution represented by the red curve.

distribution of it is

$$P\{H_{max} < h\} = e^{-\lambda(1-P\{H < h\})} \quad (1)$$

where $P\{H < h\}$ is the probability distribution of the storm surge. Then, by definition, the surge return period T is

$$T = \frac{1}{1 - P\{H_{max} < h\}} \quad (2)$$

Equation (2) may also be solved for the return level h , given a return period T . In our case, we model the tail of the surge distribution with a Generalized Pareto Distribution (GPD),

$$P\{H < h\} = 1 - \zeta_u \left[1 + \xi \left(\frac{h - u}{\sigma} \right) \right]^{-1/\xi} \quad (3)$$

where u is a large threshold, ζ_u is the probability that the surge exceeds u , and ξ and σ are the shape and location parameters of the GPD, respectively. Then the return level h ($h > u$) is calculated as

$$h = u + \frac{\sigma}{\xi} \left\{ \left[- \frac{\lambda \zeta_u}{\log\left(1 - \frac{1}{T}\right)} \right]^\xi - 1 \right\} \quad (4)$$

The GPD parameters, and thus the expected return level curve, can be estimated by the maximum likelihood method. The associated statistical confidence interval can be calculated with the Delta method, using the estimated variance-covariance matrix of the distribution parameters³⁸. The GPD fits relatively well with the upper tail of the storm surge distribution for almost all storm sets in this study, as shown in Figs. S8 and S9.

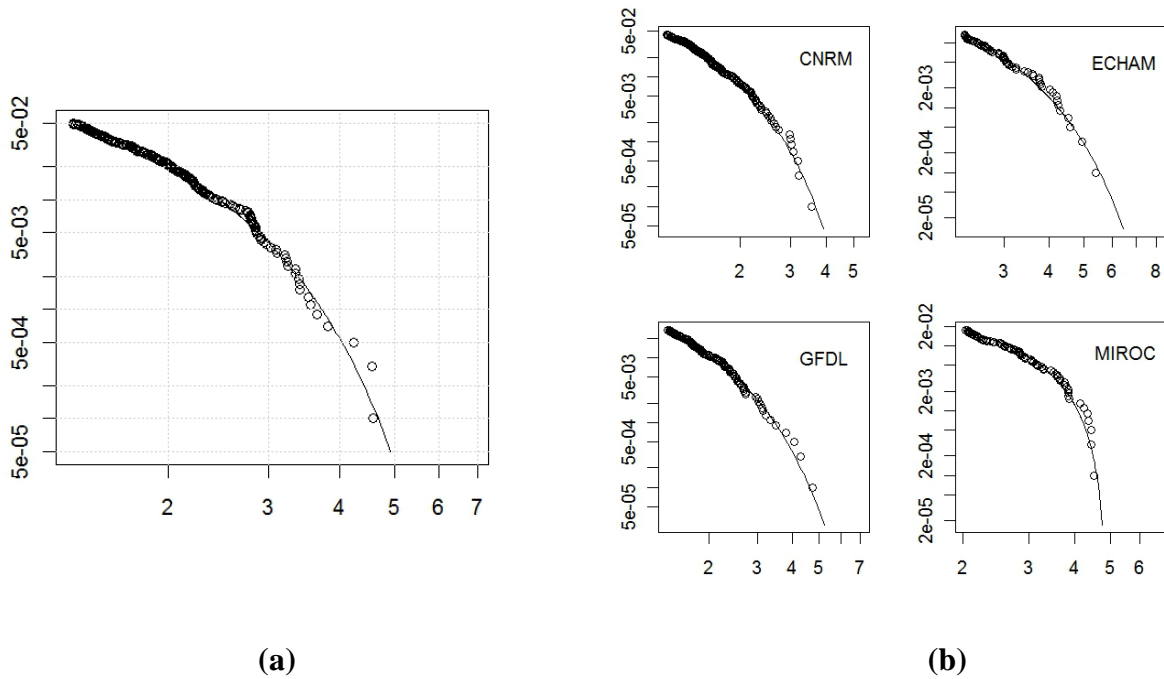


Figure S8. GPD fit of the upper tail of the storm surge distribution for the storm set under the NCEP/NCAR 1981-2000 climate condition (a) and for the storm sets under the GCM 1981-2000 climate conditions (b). The x axis is the storm surge (m) at the Battery and the y axis is the exceedance probability.

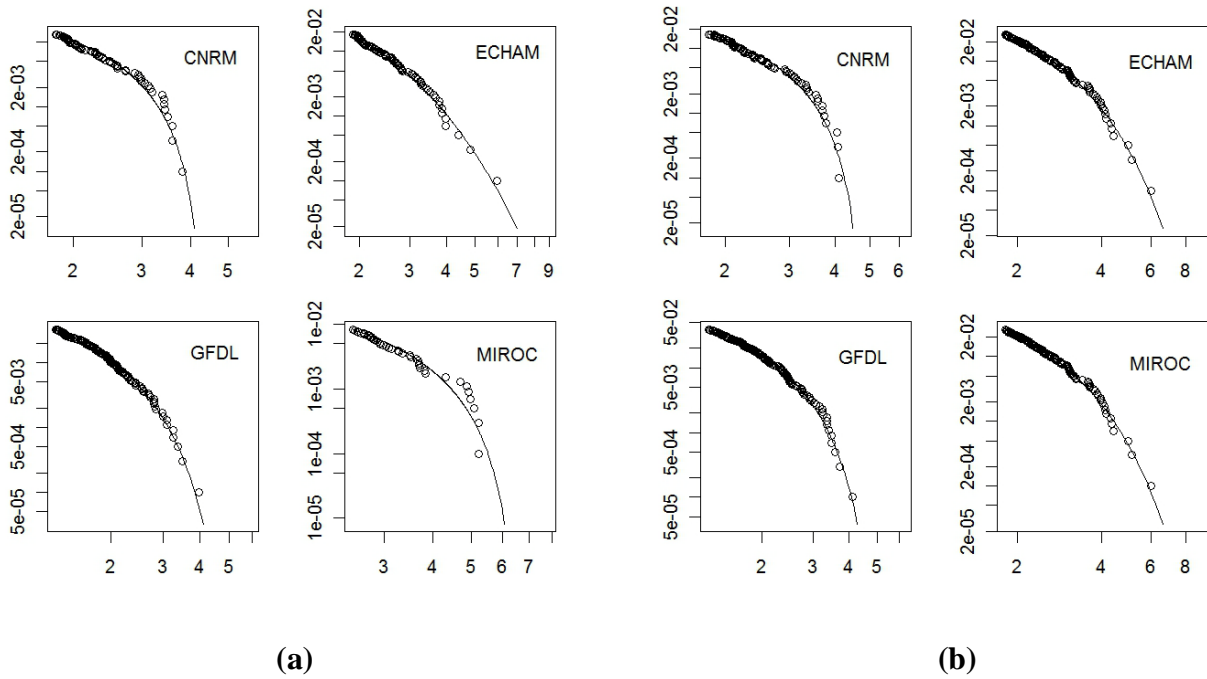


Figure S9. GPD fit of the upper tail of the storm surge distribution for the storm sets under the GCM 2081-2100 climate conditions, with storm size determined by the observed statistics (a) and with R_o increased by 10% and R_m increased by 21% (b). The x axis is the storm surge (m) at the Battery and the y axis is the exceedance probability.

ADDITIONAL REFERENCES FOR SUPPLEMENTAL MATERIAL

51. Powell, M. D., Houston, S. H., Amat, L. R. & Morisseau-Leroy, N. The HRD real-time hurricane wind analysis system. *J. Wind Eng. Ind. Aerodyn.*, **77&78**, 53-64 (1998).
52. Booij, N., Ris, R.C. & Holthuijsen, L. H. A third-generation wave model for coastal regions, 1. Model description and validation. *J. Geophys. Res.*, **104**, C4, 7649–7666 (1999).
53. Tang, Y. M., Grimshaw, R., Sanderson, B. & Holland, G. A numerical study of storm surges and tides, with application to the north Queensland coast. *J. Phys. Oceanogr.*, **26**, 2700-2711 (1996), doi: 10.1175/1520-0485(1996)026<2700:ANSOSS>2.0.CO;2.
54. Rego, J. L. & Li, C. Nonlinear terms in storm surge predictions: Effect of tide and shelf geometry with case study from Hurricane Rita. *J. Geophys. Res.*, **115**, C06020 (1999), doi: 10.1029/2009JC005285.
55. Rumpf, J., Weindl, H., Höpfe, P., Rauch, E. & Schmidt, V. Stochastic modeling of tropical cyclone tracks. *Math Meth Oper Res*, **66**, 3, 475–490 (2007).
56. Rumpf, J., Weindl, H., Höpfe, P., Rauch, E. & Schmidt, V. Tropical cyclone hazard assessment using model-based track simulation. *Nat. Hazards*, **48**, 383-398 (2009).
57. Elsner, J. B. & Bossak, B. H. Bayesian analysis of U.S. hurricane climate. *J. Climate*, **14**, 4341-4350 (2001).